A SIMPLE POROELASTIC-BASED ALGORITHM FOR EVALUATING ANOMALOUS FLUID PRESSURE ATTRIBUTED TO SURFACE LOADING: CASE STUDY OF MICHIGAN BASIN GLACIATION

by

Yonas T. Tsegay

A thesis submitted to the faculty of
The University of Utah
in partial fulfillment of the requirements for the degree of

Master of Science

Department of Civil and Environmental Engineering

The University of Utah

December 2016

The University of Utah Graduate School

STATEMENT OF THESIS APPROVAL

The thesis of **Yonas T. Tsegay**

has been approved by the following supervisory committee members:

Brian James McPherson	, Chair	**10/24/2016**
		Date Approved
P. K. Andy Hong	, Member	**10/24/2016**
		Date Approved
Christine A. Pomeroy	, Member	**10/24/2016**
		Date Approved

and by **Michael E. Barber** , Chair/Dean of

the Department/College/School of **Civil and Environmental Engineering**

and by David B. Kieda, Dean of The Graduate School.

ABSTRACT

In Michigan and surrounding states, anomalous high fluid pressures at depth are attributed to Pleistocene glaciation. Specifically, surface loading of ice and glacial till is hypothesized to compact deep subsurface sediments, and low hydraulic diffusivity of those sediments may require 10^5 years or longer to equilibrate. Given that the last major glaciation was the Wisconsin glaciation approximately 35,000 years ago, the primary hypothesis tested is whether this conceptual model may explain observed overpressures in the Michigan Basin. The objective of this study was to assemble a meaningful poroelastic algorithm to simulate and quantify the impacts of stress (force) induced by Pleistocene glaciers on deep subsurface fluid pressures. We implemented the simple algorithm in a conventional groundwater flow simulator (TOUGH2, a geothermal reservoir simulator developed by Lawrence Berkeley National Laboratory). Simulation results suggest that excess head may be generated by glacial loading, but for either permeability at the lower end of the range (10^{-16} m^2 or less, approximately), or for ice-loading rates at the upper possible range (approaching 2 cm/year during glaciation).

CONTENTS

ACKNOWLEDGMENTS

First of all, I praise God the almighty for providing me this opportunity and granting me the capability to proceed successfully. This thesis paper appears in its current form due to the assistance and guidance of Dr. Brian McPherson. I would therefore like to offer my sincere thanks to Dr. Brian McPherson and my family.

CHAPTER 1

INTRODUCTION AND SCOPE

Like many other sedimentary basins within the continental U.S., the Michigan Basin has been the subject of extensive geologic studies, primarily because of its economic resources, including oil and gas (Hake, 1938), ores (Reed, 1991), gypsum and other building materials (Carlson, 1964). Much of the data available for the Michigan Basin are from oil and gas exploration, especially data for the deeper portions of the basin. Studies of groundwater hydrology, especially deep basin hydrodynamics, are not extensive. Our initial intent for studying the deep hydrology of the Michigan Basin was to characterize flow conditions along the southern boundary of the basin, ultimately to establish boundary conditions for a companion study of the basins and arches region of Indiana, Ohio, and the Appalachian Basin. A recent study by Gupta and Bair (1997) focused on this region for the sake of characterizing the potential of specific reservoirs for hazardous liquid waste disposal.

Gupta and Bair (1997) evaluated regional-scale hydrodynamics of the southern Michigan Basin using a steady-state, variable density fluid flow model. Directions of their simulated variable density flow are 180^{o} different than simulated flow driven by topography alone. Bahr et al. (1993) characterized observed anomalously high fluid pressures at depth, and attributed the cause to Pleistocene glacial loading.

Our objectives are to characterize the regional-scale groundwater flow regime of the Michigan basin, and to evaluate possible mechanisms responsible for apparent

anomalous flow out of the basin towards the south. We assembled a very simplified mathematical model of the basin for study.

CHAPTER 2

GEOLOGIC SETTING

The Michigan Basin is roughly circular in map view and filled by nearly 4.5 km of Cambrian through Jurassic strata. Middle Proterozoic rift-related sedimentary rocks underlie the Phanerozoic succession in the northern peninsula and along a northwest-southeast trending band across the southern peninsula. Northwest-southeast trending faults and folds parallel the trend of the rift basin. Pleistocene glacial till unconformably overlies the Phanerozoic succession. These poorly consolidated sands, gravels, and clays reach a maximum of 360 m, but across most of the area are less than 120 m thick (Bergquist, 1933). Bergquist (1933) inferred that these glacial sheets exceeded 5000 feet in thickness, but given that confirmation of a specific thickness was not achieved, we elected to use the known minimum thickeness of the till deposits (360 m).

Basin-fill strata are grouped into hydrostratigraphic units following Catacasinos et al. (1990), Catacosinos and Daniels (1991), Gupta and Bair (1997), and Bahr (1993) (Table 1). Cambrian through lower Ordovician basin fill consists of shallow marine sedimentary rocks, including 3 laterally extensive layers of relatively high permeability sandstone (Mount Simon, Galesville, and St. Peter formations), separated by low permeability, heterogeneous strata composed of interbedded shale, siltstone, dolostone, and glauconitic sandstone (Eau Claire and Franconia formations). The Trempleau-Prairie du Chien Group and the Glenwood Formation, which lie immediately above and below the St. Peter Sandstone, also form layers of mixed lithology, heterogeneous strata.

Middle and upper Ordovician Trenton and Black River limestones form a relatively thick (>300 m) and homogeneous succession of fine-grained, deeper marine carbonate (Budai and Wilson, 1991). They grade upward into low permeability shale that constitutes much of the Orodvician to Silurian Utica Shale and the Middle to Upper Silurian Niagara Formation. Isolated pinnacle reefs and barrier reefs in the Niagara Formation form a higher permeability dolomite rim around the basin center (Friedman and Kopaska-Merkel, 1991).

The Upper Silurian Salina Group consists of evaporite layers, up to 145 m thick, interbedded with layers of dolostone and shale. Evaporite minerals include anhydrite and, near the basin center, halite and sylvinite. They are skirted by carbonate around the basin rim. These thick halite layers are a potential source for high-density brine in the basin, which Gupta and Bair (1997) suggested generate density-driven, updip flow.

The Upper Silurian Bass Islands Group and the Devonian strata of the Michigan basin constitute a thick low permeability succession consisting of shale, carbonate, evaporite, and locally developed sandstone rock units. Mississippian and Pennsylvanian strata consist of marginal marine and nonmarine sandstone, shale, carbonate, and coal. They are overlain by Jurassic sandstone and shale only in the center of the basin.

Table 1 summarizes ranges of values of parameters required to simulate ice (surface) loading and associated fluid pressure effects.

Symbol	Data Type	Typical Value
ϕ	Porosity	ranges from <1% to 20%
Z	Depth	ranges from 1500m to 3500m and 335m at center
k	Permeability	ranges from $10^{-14}m^2$ to $10^{-10}m^2$
ϱ_l	Fluid density,	ranges from 1000 kg/m^3 to1160 kg/m^3
ϱ_s	Solid matrix density	ranges from 2200 kg/m^3 to 2800 kg/m^3
μ	Dynamic viscosity	$1.002*10^{-3}Ns/m^2$ to $1.008*10^{-3}Ns/m^2$
u^l	Fluid velocity	ranges from $3.53*10^{-4}m^2$ to $7*10^{-4}m^2$
u^s	Solid matrix velocity	ranges from $7.0*10^{-8}m/s$ to $9.0*10^{-8}m/s$
K	Hydraulic conductivity	ranges from $3.53*10^{-6}$ m/s to $1.41*10^{-4}$ m/s
$\dot{m}_s$	Sedimentation rate	ranges from $7.0*10^{-8}m/s$ to $9.0*10^{-8}m/s$
g	Gravitational acceleration	$9.81m/s^2$
t	Time	25,000years
G	Shear modulus	ranges from $10*10^9Pa$ to $20*10^9Pa$
a	grain to grain contact surface area per unit (grain) area	0.2 – 0.3
$\sigma_1, \sigma_2, \sigma_3$	Stress tensors	
p_e	Effective pressure	
α	Compressibility of solid	
β	Compressibility of water	

CHAPTER 3

OBSERVED HYDRODYNAMICS AND FLUID PRESSURES

Groundwater hydrology of the Michigan Basin is characterized well, at least for younger sediments in the basin. The U.S. Geological Survey conducted a limited study of the basin in their Regional Aquifer System Analysis (RASA) program, including studies by Swain (1986), Baltusis et al. (1992), and Hoaglund (1996, 1998), among others. Other studies have focused on the shallow aquifers of the basin and their interaction with lakes, e.g., Kolak et al. [1995]. One study of deeper units was performed by Mandle and Knotis [1992] of the U.S.G.S., who simulated groundwater flow in the Cambrian-Ordovician aquifers of the basin (Table 1), using a 3-dimensional model.

More recent studies of the deeper Michigan Basin hydrodynamics identified regions of anomalously high fluid pressures and/or seemingly anomalous flow directions in the basin deep. Gupta and Bair (1997) evaluated the regional-scale hydrodynamic regime of the midcontinent basins and arches region, including the southern Michigan Basin and eastern Illinois Basin, western Appalachian Basin, and the arches region in between all three basins. Results of their steady-state, variable density fluid flow model suggest that saline groundwater within the Mt. Simon Sandstone flows from the deepest part of the basin towards the basin rim to the south (Figure 1a). Gupta and Bair (1997) attribute this apparently anomalous deep flow to sinking of brines from the Silurian evaporites above, i.e., sinking of higher density fluids effectively drives lower density groundwater flow from

depth. This result is contrary to that suggested by a model of topographically driven groundwater flow (no salinity).

Another study by Bahr et al. (1993) characterized observed anomalously high fluid pressures within the Glenwood Formation and St. Peter Sandstone. Observed hydraulic head values in the St. Peter Sandstone are as much as 200 m in excess of surface topography, as illustrated in Figure 1b. Bahr et al. (1993) inferred glacial loading during the past 2 My to increase fluid pressures much like rapid sedimentation increases fluid pressures (e.g., Gulf coast type hydrodynamics). They further interpreted maintenance of such high fluid pressures to present day to be possible only in relatively low permeability formations or formations with bounding formations of very low permeability.

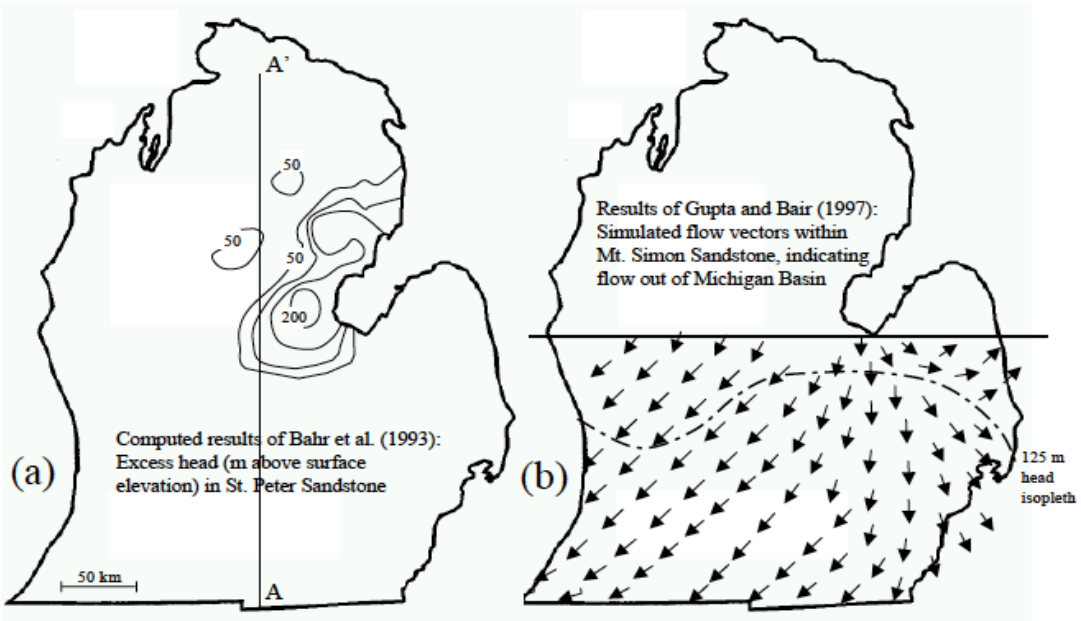

Figure 1. Observed hydrodynamic regimes within (a) the St. Peter Sandstone, and (b) the Mt. Simon Sandstone. Bahr et al. (1993) attribute observed anomalous (excess) hydraulic head values in the St. Peter Sandstone (a) to Pleistocene glacial loading. Gupta and Bair (1997) attribute modeled flow directions in the Mt. Simon Sandstone to variable density brine flow; flow directions are inferred to be anomalous compared to what topographically driven flow would suggest. Horizontal line on (b) indicates northernmost boundary of Gupta and Bair (1997) model. Location of profile A - A' is indicated on left map. (adapted from Bahr et al., 1993)

CHAPTER 4

ALTERNATIVE HYPOTHESIS: GLACIAL LOADING VERSUS SINKING OF VARIABLE DENSITY BRINE

Our objectives are to characterize the regional-scale groundwater flow regime of the Michigan basin, with a specific objective of evaluating two possible hypotheses concerning the cause of apparent high fluid pressures and anomalous flow out of the basin towards the south:

1. Pleistocene glacial loading, including 360 m of glacial materials (Catacosinos et al., 1990) deposited during the past 2 My, and
2. Sinking of high density brines from the Silurian Salina Group to deeper formations, causing lower density groundwater flow at depth.

This thesis provides results of testing only the former hypothesis, specifically whether Pleistocene glacial loading can be ruled out as an overpressure mechanism.

CHAPTER 5

HYPOTHESIS TESTING: MICHIGAN BASIN REGIONAL-SCALE MODEL

5.1 Model Description

A two-dimensional finite volume model of the Michigan Basin cross-section A-A' (location illustrated on Figure 1) is used for the simulations. The model domain is 388 km horizontal by 4.8 km vertical, consisting of 910 grid-blocks (65 columns of 14 rows), each 5.97 km by 1 m wide, and thickness/height determined by structural stratigraphy. The primary finite volume grid used is depicted in Figure 2. Below this primary mesh are 20 additional rows of finite difference cells, used only to facilitate emplacement of heat flow boundary conditions at 50 km below the basin and a proper transient thermal response. Such distance is necessary to properly simulate the transient thermal response of basin strata to changes in surface temperature and other conditions (McPherson and Bredehoeft, 2001).

The 13 hydrostratigraphic model units simulated are summarized in Table 1. We elected to use a 2-dimensional model, rather than a 3-dimensional model, primarily because it was easier to assemble and execute. More importantly, because a 2-dimensional model eliminates fluid flow into the third dimension, development of high fluid pressures will be maximized, at least compared to a 3-dimensional model. Thus, we reason that a 2-dimensional model will simplify evaluation of glacial loading effects on fluid pressures.

The computer code TOUGH2, developed and detailed by Pruess (1991), which includes coupled flow of heat, groundwater, and brine, was used to carry out all simulations

of glacial loading, with added implementation of the following algorithm for invoking a fluid pressure response to loading.

5.2 Stress by Ice Loading: General Algorithm

We considered a conceptual model to be as simple as an ice block resting on a solid matrix (Figure 2). With time, the solid matrix get compressed elastically and the porosity ϕ also behaves elastically as a function of effective pressure p_e. The flow path of both solid and liquid phases in the model is assumed to be 1-dimensional, lateral flow path being assumed negligible. For the given model, b(t) is the basin basement and h(t) is the ocean floor level. The algorithm for the 1-dimensional compaction can be written as follows.

Terzaghi's relation of effective pressure:

$$p_e = \sigma_T - p \tag{1}$$

Mass conservation:

$$\frac{\partial \emptyset}{\partial t} + \frac{\partial}{\partial z}(\emptyset u^l) = 0 \tag{2}$$

$$-\frac{\partial \emptyset}{\partial t} + \frac{\partial}{\partial z}[(1-\emptyset)u^s] = 0 \tag{3}$$

Darcy's law:

$$\emptyset(u^l - u^s) = -\frac{k}{\mu}\left(\frac{\partial p}{\partial z} + \rho_l g\right) \tag{4}$$

Force balance:

$$\nabla \cdot \sigma_e - \nabla \cdot p + \rho g = 0 \tag{5}$$

In the given equations, u^l and u^s represent the velocities of fluid and solid matrix, k and μ being the matrix permeability and liquid viscosity respectively, and g the gravitational acceleration.

Rheological constitutive relationship:

$$\sigma_e = 2G\epsilon - (p_e + \tfrac{2}{3}G\nabla \cdot U)\delta \quad (6)$$

having constitutive relationship of effective pressure:

$$p_e = p_e(\emptyset) \quad (7)$$

$$\frac{d\sigma_e}{dt} = -K\nabla \cdot u^s \quad (8)$$

$$\frac{d\sigma_e}{dt} = 2G\dot{\epsilon} - (\dot{pe} + \tfrac{2}{3}G\nabla \cdot u^s)\delta \quad (9)$$

The effective stress tensor is of the diagonal form

$$\sigma_e = \ diag\ (-\sigma_1, -\sigma_{3,} - \sigma_3) \quad (10)$$

Thus (4) becomes

$$-\frac{\boldsymbol{\partial \sigma_3}}{\boldsymbol{\partial z}} - \frac{\boldsymbol{\partial p}}{\boldsymbol{\partial z}} - [\rho_s(1-\emptyset) + \ \rho_l\emptyset]g \ = 0 \quad (11)$$

If elastic law is assumed (7) and (8), the diagonal components of the stress tensor becomes

$$-\sigma_1 \ = -(\dot{pe} + \tfrac{2}{3}G\frac{\partial u^s}{\partial z}) \quad (12)$$

$$-\sigma_3 \ = -\dot{pe} + \tfrac{4}{3}G\frac{\partial u^s}{\partial z} \quad (13)$$

From the relation $\dot{pe} = \ -K\frac{\partial u^s}{\partial z}$ (14)

$$\sigma_1 \ = (1 - \frac{2G}{3K})p_e \quad (15)$$

$$\sigma_3 \ = (1 + \frac{4G}{3K})p_e \quad (16)$$

σ_3 being the vertical component of the stress.

Terzaghi's (1) relation can be modified via Skempton (1960).

$$p_e = \sigma_T - (1-a)p \quad (17)$$

a being grain to grain contact surface area per unit (grain) area.

From (11), a simplified equation can be written as:

$$-(1+\tfrac{4G}{3K})\frac{\partial p_e}{\partial z}-(1-a)\frac{\partial p}{\partial z}-[\rho_s(1-\emptyset)+\rho_l\emptyset]g=0 \quad (18)$$

Boundary conditions:

The natural boundary conditions are the kinematic boundary conditions at z = b,

$$u^s = u^l = \dot{b} \quad (19)$$

and a kinematic condition at z = h,

$$\dot{h} = \dot{m}_s + u^s \quad (20)$$

where $\dot{m}_s$ is the compaction rate at z=h. Also at z=h,

$$\emptyset = \emptyset_o\ ,\quad p = p_o \quad (21)$$

Nondimensionalization:

The length can be defined by length-scale *d* by writing

$$(1+\tfrac{4G}{3K})p_e = (\rho_s-\rho_l)gd(1-a)\tilde{p}(\emptyset) \quad (22)$$

Here we assume that G/K is constant. We scaled *z* with *d*, solid matrix velocity u^s with $\dot{m}_s$, time *t* with $d/\dot{m}_s$, pore pressure *p* with $(p_s-p_l)gd$, and permeability *k* with *ko*:

$$z = dz*$$

$$u^s = mo_s\dot{u}^s*$$

$$u^l = m0_s\dot{u}^l*$$

$$t = \left(\frac{d}{m\dot{o}_s}\right)t*$$

$$\dot{m}_s = m\dot{o}_s\dot{m*}_s$$

$$p = (p_s-p_l)gd*$$

$$k = k_o\tilde{k} \quad (23)$$

These variables are substituted into the equations, which then become the equations (24-26) on dropping the asterisks,

$$\frac{\partial \emptyset}{\partial t} + \frac{\partial}{\partial z}[(1-\emptyset)u^s)] = 0 \quad (24)$$

$$\frac{\partial \emptyset}{\partial t} + \frac{\partial}{\partial z}(\emptyset u^l) = 0 \quad (25)$$

$$\emptyset(u^l - u^s) = -\lambda \check{k}(\frac{\partial p}{\partial z} + r) \quad (26)$$

where

$$\lambda = \frac{k_o(\rho_s - \rho_l)g}{\mu \dot{m}_s}, \quad r = \frac{\rho_l}{\rho_s - \rho_l}$$

$$u^s = \dot{b} + \lambda \check{k}(\frac{\partial p}{\partial z} + r) \quad (27)$$

The constitutive relation of permeability and porosity is given by Smith (1971)

$$k(\emptyset) = (\emptyset/\emptyset o)^m, \text{ m=8}$$

Smith (1971) derived the equation (nonlinear compaction model) which took into account the dependence of permeabilityon porosity and the dependence of water viscosity on salinity, temperature, and pressure.

Formulating the compaction relation

$$\frac{\partial \emptyset}{\partial t} = \lambda \frac{\partial}{\partial z}\{(1-\emptyset)\left(\frac{\emptyset}{\emptyset o}\right)^8 \left(\frac{\partial p}{\partial z} + r\right)\} = 0 \quad (28)$$

and

$$\text{p} = \ln \frac{\emptyset 0}{\emptyset} - (\emptyset o - \emptyset) \text{ given by Fowler and Yang (1998).}$$

Another more common way to state equation (28) is as a function of effective stress, which facilitates expression of how pressure p changes through time, or

$$\frac{\partial \emptyset}{\partial t} = -\alpha(1-\emptyset)(\frac{\partial \sigma_e}{\partial t}) \quad (29)$$

We then combined equations (28) and (29) with an equation for density change,

$$\frac{\partial \varrho}{\partial t} = \beta \varrho (\frac{\partial p}{\partial t}) \quad (30)$$

and with an expression for change in compaction (Δz),

$$\frac{\partial (\Delta z)}{\partial t} = -\alpha \Delta z (\frac{\partial (\sigma_e)}{\partial t}) \quad (31)$$

and finally with the mass conservation equation solved by most groundwater simulation codes, or

$$\frac{\partial (\Delta M)}{\partial t} = [\phi (\Delta z) \left(\frac{\partial \varrho}{\partial t}\right) + \varrho (\Delta z) \left(\frac{\partial \phi}{\partial t}\right) + \varrho \phi \left(\frac{\partial (\Delta Z)}{\partial t}\right)] \Delta x \Delta y \quad (32)$$

Separating the fundamental groundwater flow equation from (32) yields a source term that we incorporated in TOUGH2 to facilitate analysis of pressure response due to ice (mass) loading at the surface,

$$\phi \varrho \left(\beta + \frac{\alpha}{\phi}\right) \left(\frac{\partial p}{\partial Z} \frac{\partial Z}{\partial t}\right) - \varrho \alpha \left(\frac{\partial \sigma_T}{\partial t} + \frac{\partial \sigma_T}{\partial Z} \frac{\partial Z}{\partial t}\right) \quad (33)$$

Boundary and initial conditions:

1. A uniform, constant basal heat flow was applied at the basal boundary (at 50 km depth below the basin sedimentary section). We assigned the basal heat flow to be 50 mW m^{-2}, the representative value of the range of present day surface heat flow values determined by Cercone and Pollack (1991).
2. In all simulations, the surface temperature was held constant at 15° C, splitting the difference between the speculated surface temperature of 20° C in the Permian and 10° C of Holocene time (Cercone and Pollack, 1991; Speece et al., 1985). We did not explore the ramifications of a variable surface temperature history, because of poor resolution associated with estimated marine paleo-surface temperatures.

3. Constant head equal to surface topography minus 30 m was assigned at the surface of the domain throughout each history simulation (Boutt et al., 2001). Initial fluid pressures in the subsurface were hydrostatic.
4. Basement rocks below the Mt. Simon sandstone provide a low permeability barrier that justifies a no-flow boundary along the bottom of the model domain (Gupta and Bair, 1997). No-fluid-flow boundaries were assigned to the northern side (A') of the model domain (Figure 2), because of topographic symmetry. A specified fluid flow boundary was assigned along the southern boundary, based on inferred fluid fluxes in that direction (Gupta and Bair, 1997). A specified fluid flux boundary was also applied at the northern boundary, providing insignificant changes in model results.

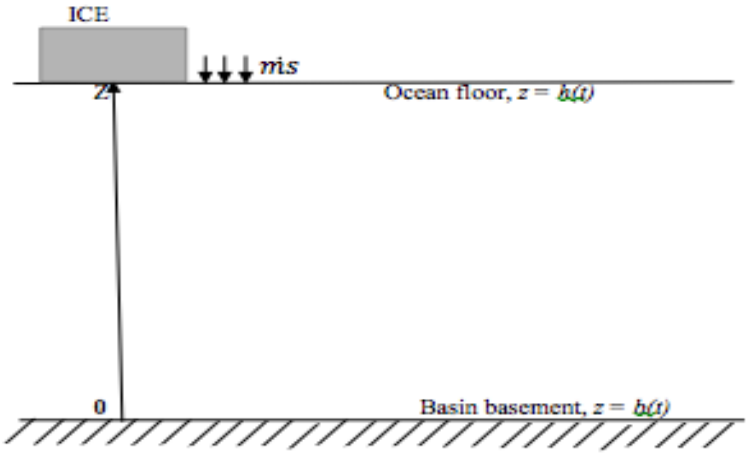

Figure 2. Schematic of conceptual model of ice (glacial) loading.

CHAPTER 6

MODEL RESULTS AND DISCUSSION

After implementing the algorithm above in TOUGH2, in particular incorporation of equations (28) – (31) and (33), a simulation was designed to test the glacial loading hypothesis of Bahr et al. (1993). The model used the mesh described above, including the permeability parameterization summarized in Table 1. The glacial loading rate we used was 180 m/My, uniformly applied over the course of 2 My, corresponding to deposition of 360 m of Tejas III glacial materials (Catacosinos et al., 1990) during the past 2 My of the Pleistocene. These loading rates are a simplified minimum, given that the thickness (and weight) of ice associated with these materials would be much greater than the 360 m. Additionally, we assume a linear loading rate of the glacial materials, also a minimum. The glacial materials were deposited only across the center section of profile A-A', from ~154 km to ~308 km distance along the profile (Figure 2), roughly corresponding to the region displaying higher pressures (Figure 1a).

These results suggest that excess head created by deposition depends strongly on rock permeability at depth. For the glacial loading rate of 180 m/My and the permeability distribution assigned in this model (Table 1), excess head at depth does develop, but only if the formation permeability is at the very low end of the possible range, approximately less than 10^{-16} m^2. This is not an unreasonable value of sandstone permeability, but even lower values are required to induce significant overpressuring.

For excess pressures to reach Bahr's observed threshold, excess pressures in the modeled St. Peter Sandstone (Figure 2) are ~200 m above surface topography. Additionally, excess heads are regional in nature, in comparison to local anomalous flow directions induced by brine-sinking (evaluated in a separate study). Simulated excess head created by glacial loading does exceed observed values (Figure 1a) of Bahr et al. (1993), but only if permeability is at the lower end of the range (10^{-16} m^2 or less, approximately). However, computer simulation models can express exactly what the modeler wishes, and thus we could adjust the glacial deposition rate to achieve an exact match, if it were needed. However, our goal is to understand the system, not replicate it.

To understand the tradeoff between glacial loading rates and in situ permeability, we conducted a brief sensitivity study, invoking a range of glacial loading rates (140 m/My to 220 m/My), over a range of in situ permeabilities of the St. Peter Sandstone (10^{-13} m^2 to 10^{-20} m^2). Figure 3 shows the simulation result where maximum overpressure simulated by the model approach 220 m equivalent hydraulic head and Figure 4 exhibits the results of this sensitivity analysis, and thus the normalized overpressure corresponding to this effectively no significant overpressure resulted for permeability values less than 10^{-16} m^2, and thus these values are not plotted. For the assumed actual glacial loading rate minimum of 180 m/My, a permeability of < 10^{-18} m^2 was required to induce maximum overpressure (e.g., normalized overpressure approximately 1.0 in Figure 4). The computed result in the Ordovician units (10,000 ft) from the simulation showed an overpressure of 34MPa and hydrostatic pressure of 31.7MPa. The vertical axis shows normalized overpressure, a ratio of simulated overpressure to the maximum simulated overpressure.

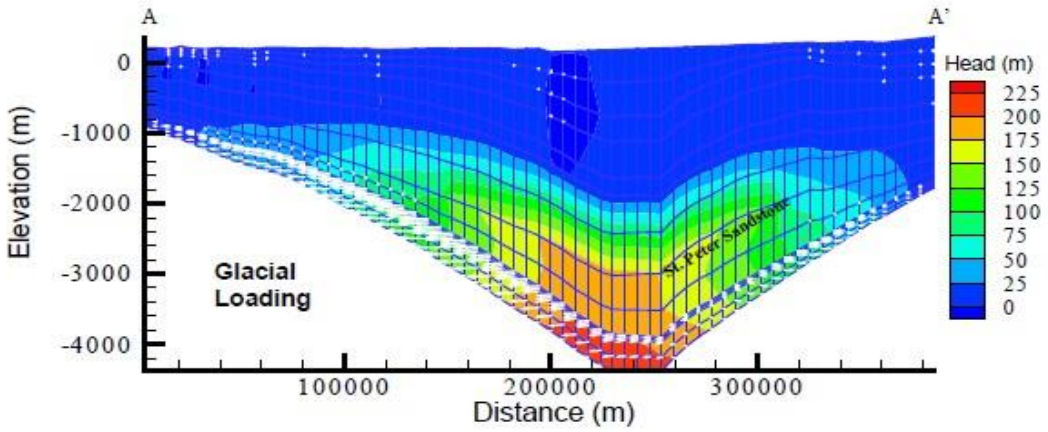

Figure 3. Simulation results of Michigan Basin glacial loading simulation: contours of excess head (head above surface topography, for comparison to Bahr et al. (1993) data and results), and flow vectors, indicating flow directions.

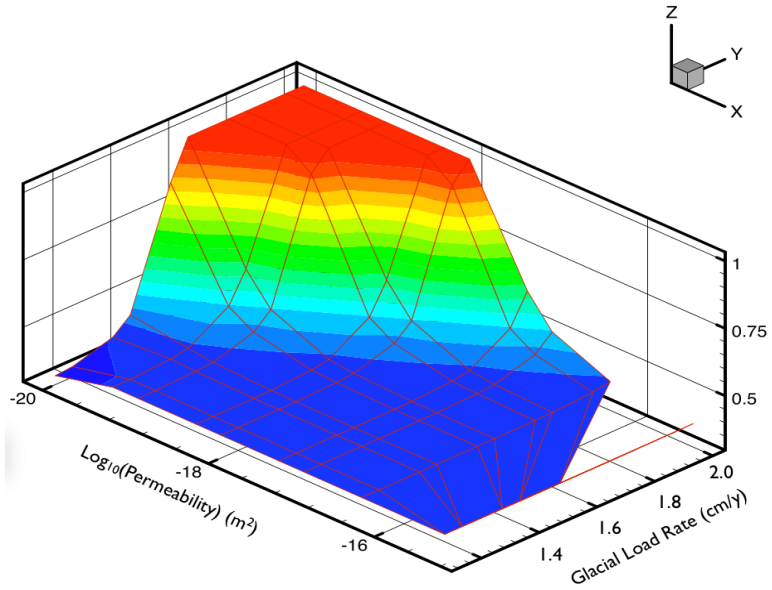

Figure 4. Results of sensitivity analysis comparing competing roles of permeability and glacial loading rate.

CHAPTER 7

SUMMARY AND CONCLUSIONS

The aim of the study was to develop an algorithm to evaluate the impact of rapid glacial surface loads on deep subsurface fluid pressures. A simple poroelastic algorithm was assembled, and a source term included in a conventional numerical groundwater simulator. Conditions specific to the Michigan Basin were evaluated as a case study, where present-day overpressures are attributed to glaciation 35,000 years ago. We designed a generalized sensitivity analysis to evaluate the relative roles of permeability and glacial loading (rates). Results of the sensitivity analysis suggest that Pleistocene glaciation may indeed be responsible for observed overpressures, albeit for lower values of sandstone permeability, less than approximately 10^{-16} m^2.

REFERENCES

Bahr, J. M., G. R. Moline, and G. C. Nadon, Anomalous pressures in the deep Michigan Basin, in *Basin Compartments and Seals, AAPG Memoir 61*, 153-165, 1994.

Baltusis, M. A., M. F. Quigley, and R. J. Mandle, Municipal ground-water development and withdrawals in the central Lower Peninsula of Michigan, 1870-1987, *U.S. Geological Surv. Open-File Rep. OF 91-0215*, 89 pp., 1992.

Bergquist, S. G., 1933, The pleistocene history of the tahquamenon and manistique drainage region of the northern peninsula of michigan; University of Michigan Ph.D. Dissertation, 37 pp.

Budai, J.M., and Wilson, J.L., Diagenetic history of the Trenton and Black River formations in the Michigan Basin, in *Early Sedimentary Evolution of the Michigan Basin, Geological Society of America Special Paper 256*, 73-88, 1991.

Carlson, E. T., Gypsum in Michigan, *Michigan Geological Survey Bulletin, 1*, 77-78. 1964.

Catacosinos, P. A., P. A. Daniels, Jr., and W. B. Harrison III, Structure, stratigraphy, and petroleum geology of the Michigan Basin, in *Interior Cratonic Basins*, *Am. Assoc. Petrol. Geol. Memoir, 51*, 561-601, 1990.

Catacosinos, P. A., and P. A. Daniels, Jr., Stratigraphy of Middle Proterozoic to Middle Ordovician formations of the Michigan Basin, in *Early Sedimentary Evolution of the Michigan Basin, Geological Society of America Special Paper 256*, 53-71, 1991.

Cercone, K. R., and H. N. Pollack, Thermal maturity of the Michigan Basin, in *Early Sedimentary Evolution of the Michigan Basin, Geological Society of America Special Paper 256*, 1-11, 1991.

Cercone, K. R., Thermal history of the Michigan Basin, *Am. Assoc. Pet. Geol. Bull., 68*, 130-136, 1984.

Clifford, M. J., Subsurface liquid-waste injection in Ohio, *Inf. Cir. 43*, 27 pp., Div. of Geol. Surv., Ohio Dep. of Nat. Resour., Columbus, 1975.

Davies, P. B., Variable-density ground-water flow and paleohydrology in the waste isolation pilot plant [WIPP] region, southeastern New Mexico, *U.S. Geol. Surv. Open File Rep. 88-490*, 139 pp., 1989.

Friedman, G.M., and Kopaska-Merkel, D.C., Late Silurian pinnacle reefs of the Michigan Basin, in *Early Sedimentary Evolution of the Michigan Basin, Geological Society of America Special Paper 256*, 89-99, 1991.

Gupta, N., Geologic and fluid-density controls on the hydrodynamics of the Mt. Simon Sandstone and overlying geologic units in Ohio and surrounding states, Ph.D. dissertation, 266 pp., Dep. of Geol. Sci., Ohio State Univ., Columbus, 1993.

Gupta, N., and E. S. Bair, Variable-density flow in the midcontinent basins and arches region of the United States, *Water Resources Res., 33*, 1785-1802, 1997.

Hake, B. F., Geologic occurrence of oil and gas in Michigan, *Am. Assoc. Pet. Geol. Bull., 22*, 393-415, 1938.

Hoaglund, J. R., III, Recharge to discharge groundwater travel times in the Michigan Basin and the effect of glacial ice loading, Ph.D. Dissertation, 274 pp., Michigan State University, East Lansing, MI, 1996.

Hoaglund, J. R., MODFLOW simulations of groundwater interactions between the Michigan Basin and the Great Lakes; modern discharge and glacial ice loading, *Abstracts with Programs – Geol. Soc. of Amer., 30*, 400, 1998.

Hubbert, M.K., and W.W. Rubey, Role of Fluid Pressure in Mechanics of Overthrust Faulting, *Geological Society of America Bulletin, 70*, 115-166, 1959.

Kolak, J. J., D. T. Long, G. J. Larson, J. Grahame, D. F. Sibley, and J. M. Matty, Interactions among formation brine, near-surface groundwater, and large lakes; a preliminary assessment, *Abstracts with Programs – Geol. Soc. of Amer., 27*, 293, 1995.

Lusczynski, N. J., Head and flow of water of variable density, *J. Geophys. Res., 66(12)*, 4247–4255, 1961.

Mandle, R. J., and A. L. Knotis, Simulation of regional ground-water flow in the Cambrian-Ordovician aquifer system in the northern Midwest, *U. S. Geol. Surv. Prof. Paper P 1405-C*, 97 pp., 1992.

Pruess, K., TOUGH2--a general-purpose numerical simulator for multiphase fluid and heat flow, *Lawrence Berkeley Laboratory Report. LBL-29400*, Lawrence Berkeley National Laboratory, Berkeley, CA, 1991.

Reed, R. C., Economic geology and history of metallic minerals in the Northern Peninsula of Michigan, in *Early Sedimentary Evolution of the Michigan Basin, Geological Society of America Special Paper 256*, 13-51, 1991.

Senger, R. K., and G. E. Fogg, Stream functions and equivalent fresh-water heads for modeling regional flow of variable-density ground-water, 2, Application and implications for modeling strategy, *Water Resour. Res., 26(9),* 2097–2106, 1990.

Sonnenfeld, P., and Al-Aasm, I., The Salina evaporties in the Michigan Basin, in *Early Sedimentary Evolution of the Michigan Basin, Geological Society of America Special Paper 256*, 89-99, 1991.

Speece, M. A., T. D. Bowen, J. L. Folcik, and H. N. Pollack, Analysis of temperatures in sedimentary basins: The Michigan Basin, *Geophysics, 50,* 1318-1334, 1985.

Swain, L. A., Michigan Basin regional aquifer-system study, *U. S. Geol. Surv. Circ., C 1002, 242-244*, 1986.

Warner, D. L., Hydrogeologic and hydrochemical assessment of the basal sandstone and overlying Paleozoic age units for wastewater injection and confinement in the north central region, Underground Injection Pract. Counc., Oklahoma City, Okla., 1988.